LAB University of Applied Sciences

LiDAR Drone Design, Weight Reduction, And Optimization

LAB University of Applied Sciences
Bachelor of Engineering, Mechanical Engineering
2024
Precious Akpata

Abstract

Author(s)	Publication type	Completion year
Precious Akpata	Thesis, UAS	2024
	Number of pages	
	29	

Title of the thesis

LiDAR Drone Design, Weight Reduction, And Optimization

Engineer (UAS), Mechanical Engineering

Abstract

The aim of this study was to investigate the feasibility of optimizing the performance of an unmanned aerial vehicle. The mission profile of the vehicle was aerial mapping using a LiDAR sensor. Drones, with the same or similar mission requirements, available in the marketplace were evaluated. The work done in the thesis used these marketplace drones as a benchmark. Further analyses, simulations, and selection criteria were used to arrive at a conclusion for the feasibility of producing a drone that exceeded the benchmarks set. It was found that manufacturing a LiDAR capable drone optimized for long duration flights, with low total weight, and cost was possible with the caveat of certain current limitations.

Keywords

Aerial Mapping, Drone, LiDAR, UAV, Gliding

Contents

List of Terms

AC	Advisory Circular
AOA (α)	Angle of Attack
C_l	Coefficient of Lift
C_m	Coefficient of Moment
C_d	Coefficient of Drag
C_{D0}	Zero Lift Drag Coefficient
C_{Df}	Fuselage Drag Coefficient
GSD	Ground Sampling Distance
NACA	National Advisory Committee on Aeronautics
LiDAR	Light Imaging Detection And Ranging
RC	Remote Control (Planes)
RTK	Real Time Kinematic
UAV	Unmanned Aerial Vehicle
V_s	Velocity of Descent, Sinking Speed

1 Introduction

Both Unmanned Aerial Vehicles (UAVs from here) and Light Imaging Detection And Ranging (LiDAR from here) are relatively old technologies that are only now becoming widely adopted. UAVs are almost as old as manned aircraft with the first successful UAV flight, the Curtiss N-9, occurring in 1916 (Abdulla Q) and LiDAR instruments about a half a century later, having been invented in 1961 by the Hughes Aircraft Company. Despite the length of time these technologies have been available, they have only just started to be widely adopted over the last two decades. UAVs in the form of rotary drones have surged in usage in both the industrial and commercial applications. LiDAR has been adopted less widely as the systems are still prohibitively expensive for most casual consumers; however, demand for LiDAR systems has grown for scientific, engineering, environmental, archaeological, and agricultural purposes. The combination of UAVs equipped with LiDAR payloads in particular is an area of growing importance. Weight, flight time, and cost are all critical issues which place limits on the application of these technologies in professional domains. These three key constraints present a circular problem: with each node of the problem feeding back to another. The researcher aims, in this study, to explore a potential design to overcome these limitations and, by so doing, demonstrate the feasibility of lightweight, long endurance, low-cost LiDAR drones. Regarding the first aim, this study is focused on providing an integrated optimized solution to the three issues by reworking the design. The constraint of flight time, in particular, was seen as advantageous to overcome as limited duration flights are a bottle neck for aerial LiDAR mission conducted by UAVs. Overcoming this impediment would help especially for missions where large scale environments are being observed.

2 Literature Review

The researcher reviewed several text-based sources to motivate the development of the study. The nature of the study is such that most of the sources were published relatively recently: within the last half decade. The sources reviewed concentrated on three key areas: drone design principles, LiDAR applications, and other remote sensor technologies.

Three separate sources helped to expand the researcher's knowledge in areas of drone design and optimization using distinct approaches. First, Optimization of quadcopter frame using generative design and comparison with DJI F450 drone frame (Bright et al 2020) took a generative design approach and focused on a specific widely available brand drone. Generative design is an approach to concept development / prototyping that utilizes proprietary machine learning algorithms in conjunction with cloud computing to rapidly produce multiple iterations of potential designs. The research paper, Novel Drone Design Using an Optimization Software with 3D Model, Simulation, and Fabrication in Drone Systems Research introduced FEA applications using the software 3DEXPERIENCE. Finally, Design and Development of Unibody Quadcopter Structure Using Optimization and Additive Manufacturing Techniques focused on drone design from a production technology standpoint. In particular, it introduced the researcher to new additive manufacturing concepts.

USA Imagery's web-based article on LiDAR technology and associated terminology helped the researcher to gain a solid foundational understanding of LiDAR systems and their usage. Airborne LiDAR Technology: A Review of Data Collection and Processing Systems (Lohani & Ghosh) furthered that understanding and expanded it to a more academic level. While Challenges and Opportunities in Lidar Remote Sensing. Frontiers (Menenti & Zhein 2021) investigated the limitations of the technology and helped the researcher to gain insight into potential opportunities for optimization.

Depth Sensing Beyond LiDAR Range (Zhang et al 2020) focused on techniques, technologies, and procedures to work around the limitations of LiDAR particularly in the domain of autonomous driving. Onboard Detection and Localization of Drones Using Depth Maps (Carrio et al 2020) evaluated to application of Depth Maps sensors for drone flight and collision detection. The researcher investigated this topic as Zed cameras, incorporate several pieces of pieces of equipment that are also used in LiDAR systems into a more compact frame.

Each piece of literature helped the researcher to gain a clearer understanding of the study. Nonetheless, the work developed here is rather distinct from most of the literature reviewed as the researcher took a different approach to solving the problem. One limitation of this

literature review is that few papers and books on the field of traditional aerospace engineering were reviewed; however, other resources, such as seminars, and lecture recordings were used to fill in the gap.

3 Empirical Study

3.1 Concept and Development

To achieve the aims set forth in the introduction, the researcher made the decision to develop a hybrid aerial system. Most commonly, unmanned aerial systems follow one of two main morphologies: winged platforms and rotary platforms. Winged platforms tend to provide optimal flight time and altitude, whereas rotary platforms provide excellent manoeuvrability. Both features can be seen as advantageous for LiDAR mapping. Flight times of sizable duration and high altitudes can be seen as favorable for aerial mapping on large projects with geometry that is uniform or simple: such as warehouses or large agricultural plots. High manoeuvrability has been demonstrated to be an asset for smaller projects; especially if they contain features with nonuniform or complex geometry: such smaller niche construction projects or gas and electric plants. Unfortunately, both desirable features tend to come at the expense of the other. By combining the two, into a third transition, platform it was seen as possible to mitigate the cost to both features, to an extent, while maintaining the benefits. That is, the key challenge to overcome was the difficulty in successfully hybridizing these features into a working unit. It should be noted that other transition / hybrid drone platforms have been developed for a variety of purposes: including military, law enforcement, and search and rescue. This study represents the work of the author, as a focused attempt at optimizing specifically for LiDAR mapping, primarily for academic purposes.

To begin, the researcher conducted an analysis of some of the main UAVs dedicated to LiDAR mapping, currently available. This analysis, present in the Appendix 1 Table 1., helped to create a preliminary guide for target deliverables for the project. From this analysis, the decision was made to focus primarily on increasing flight time to compete with some high-end UAVs. The mean flight time from a sample of 19 units was found to 2.82×10^3 seconds. A deliverable flight time of 3.60×10^3 seconds, or one hour, was set in response. The average payload deliverable was found to be 3.88 kg. In response a target payload of 3 kg was set. Close to 75% of the UAVs available followed a multirotor morphology; however, they accounted for only 40% of the UAVs with a flight time equal to or greater than one hour. This helped to inform the decision to design a hybrid UAV. It should be noted that fixed wing craft only accounted for 20% the morphologies of UAVs with a desirable flight time, with unary rotors (Helicopters) accounting for 40%. Hybridizing between multirotor and fixed wing morphologies was selected for two main reasons, from the comparative analysis. First, the flight time represented by the fixed wing craft was considerably higher than any helicopter found in the brief study. Second, hybridizing a multirotor with a helicopter is not particularly feasible or necessary, given the nature of those two morphologies.

Another consideration was cost. The total both shaped the development of overall design and the selection of structural materials and cost. The aim was to provide a platform capable of delivering high performance capabilities, while being produced at a cost much lower than the average price point of similarly capable drones. The average price for the LiDAR focused UAVs compared was found to be approximately $14 900.00 or € 14 300.00 (see appendix I). For UAVs with the target flight times, the mean cost grew to $27 200.00 or € 26 100.00. Consequently, the researcher aimed to produce a drone at a production cost significantly lower than the averages. An aim of approximately € 7 000.00 was set as a production cost. This research was being conducted in the field of mechanical engineering and not a business or accounting field; therefore, the researcher recognized that the figure set may not quite represent the final end-user price in a production scenario. However, the aim was to achieve a price significantly lower than expected, so as to account for any potential markups. As discussed in the introduction, the driving goal of this research was to find an aerial LiDAR solution suitable for professional and academic fields. The physical features of the UAV were the primary focus, but cost was also a consideration: especially, in support of academics in fields with low funding.

3.2 Wing Design Overview

To achieve a significantly longer flight times than the most common and popular rotary UAV's, used for LiDAR surveys, the researcher decided to incorporate a wing section in conjunction with the rotors. The aim of adding the wing was to increase native aerodynamic effectiveness, particularly in terms of coefficient of lift. This was hypothesized to be a simple mechanical way to overcoming deficiencies in mission duration. However, the addition of the wing section to the overall airframe introduced its own challenges: specifically, the wing sections would need to be sized correctly, and a suitable airfoil would need to be selected. Furthermore, structural components were required to be designed for 3D printing and materials selected. Despite in inclusion the wing and the extra engineering challenges that it presented; the advantages outweighed the disadvantages.

3.3 Wing Sizing

In the process of designing the wing, first the required dimensions based on the total load of the UAV with payload considered. Following this, an airfoil optimized to increase lift, was selected. For dimensioning the wing sections the geometric parameters of area and length were focused on. The area of the wing, denoted by here by S, was found using the following equation

$$S = \left(\frac{\frac{(W_{Total} \times 10^3)}{F_{WL}}}{100} \right) \quad (1)$$

Where W_{Total} represents to total weight of the UAV, including payload and F_{WL}, or the wing loading, represents the expected force exerted on each square meter of the wing. Here, an estimate of 37 was taken for the wing load and the total mass was determined to be 3.23 kg from the summation of the UAV's components and structure. From this an area of 0.873 m^2 was found. It should be noted that based on conventions, the area found here is not the total surface area of the wing, but rather the flat surface area taken from the top projection. Following the this, the semispan, that is the length of each wing taken from root to tip, could be found. First it important to briefly discuss the concepts of aspect ratio and mean aerodynamic chord.

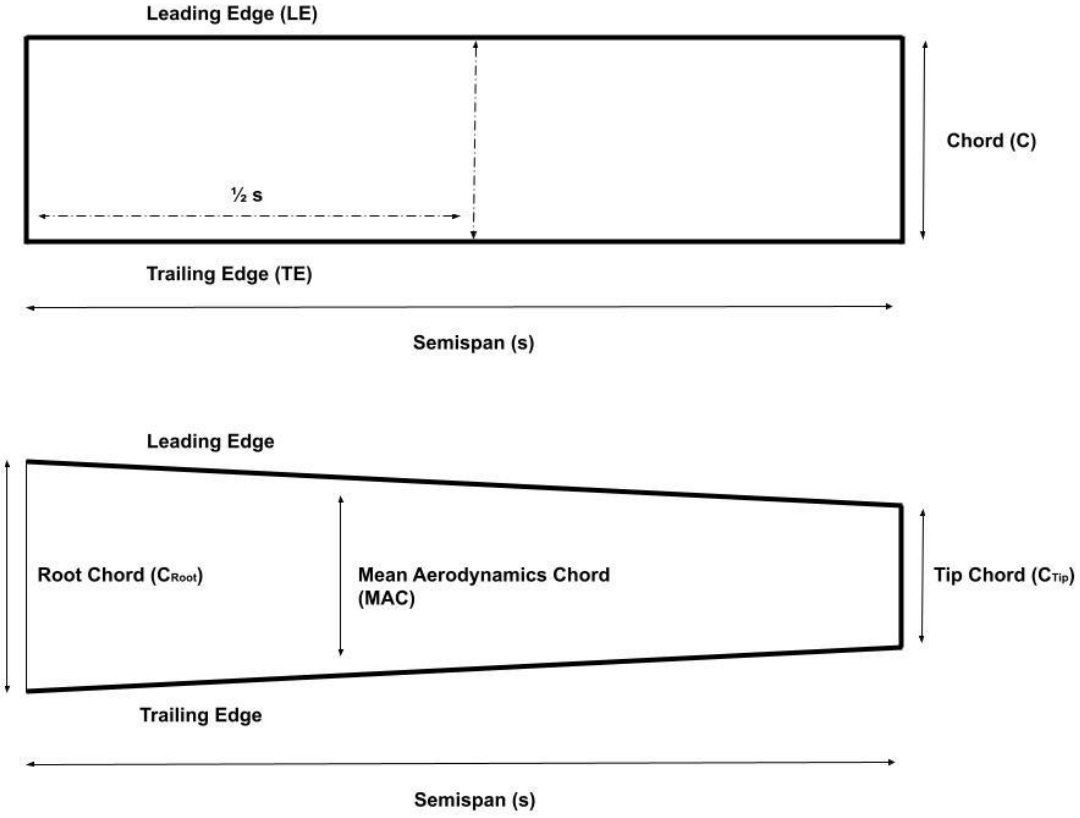

Figure 1: Plane Wing Top View Diagram (Figure: Precious Akpata)

The aspect ratio delimits the relationship between the length and breadth of a wing. The length of a single wing from root to tip, as mentioned above is referred to as the semispan. The breadth of a wing from the front edge to the trailing edge is defined as the chord or in

the case of non-uniform sections, the mean aerodynamic chord. In this study a uniform rectangular wing was utilized. Hence, the equation for the semispan of a wing is given by

$$s = \frac{1}{2}\sqrt{AR \times S} \tag{2}$$

Where s is the semispan, AR is the aspect ratio, and S is the area. From this a value of 1.477 m was found. In order to verify the results, a second approach was applied. This approach was referred to as the cubic wing loading or CWL (Durmus S 2020) and has often been used for the development of RC planes. It was seen as useful to cross reference this method as RC plane design has overlaps with modern UAV designs. Using this method requires referring to a general reference for known cubic wing loading values for specific types of flight parameters. For RC planes within gliding or sailing parameters a cubic wing load or C value of 4 can be taken (Meyers K 2018). From this we evaluate the CWL formula and arrive at a given lifting area for the aircraft.

$$C = \frac{W_{Totsl}}{S^{3/2}} \tag{3}$$

$$S = \left(\frac{W_{Total}}{C}\right)^{2/3} \tag{4}$$

Using equation (3) a value of 0.867 m^2 was found for the wing area. Hence, applying equation (4) we arrive at a semispan of 1.472 m. This was seen to be reasonable as the CWL method is often used more so for estimations rather than rigorous design.

Initially a semispan of 1.47m was considered to be quite large and undesirable for two principal reasons. First, the aim of this study was to investigate the feasibility of an affordable 3D printed LiDAR drone. Such a large size of wing would exclude most readily available and affordable 3D printers, thus reducing the feasibility in most cases. Second, the aim was to develop this UAV with the aim of field research or professional work in mind: such as archaeological studies, civil engineering as-build data generation, and forestry. A larger size could introduce difficulties for conducting such work. However, it was decided, given the simple rectangular geometry of the wing that it could be possible to combine 3D printing the wing in two or three smaller subsections with snap-fit fastener mechanisms to form the complete wing structure. This would also allow the drone to be assembled and disassembled quickly and easily in the field, when necessary.

3.4 Air Foil Selection and Analysis

A critical component of designing any aerodynamic machine element is selecting an airfoil to achieve specific aerodynamic qualities. An airfoil is a geometric representation of the cross section of an aerodynamic machine element such as a wing, propeller, or turbine. There are numerous types of airfoils available to choose from. Airfoils are typically grouped into specific series. One of the most well-established series of airfoils are the NACA (National Advisory Committee on Aeronautics) series. There are two primary subseries of NACA airfoils defined as series 4 and 5 respectively. The researcher chose to focus on NACA series 4 for the selection of an airfoil for the drone's wings. The reason for this being the ease of use with a variety of aerodynamics analysis software. Airfoils were not selected for the drone's propellers as the researcher made the decision to select from manufactured propellers, whereas the wings would be designed and 3D printed independently.

NACA series 4 airfoils are defined in a specific way. First, here we will introduce the key properties of all airfoils. Next, we will discuss how NACA 4 are defined, using these universal properties. The key properties that must be considered when defining an airfoil are chord, camber, leading edge, trailing edge, upper surface, and lower surface.

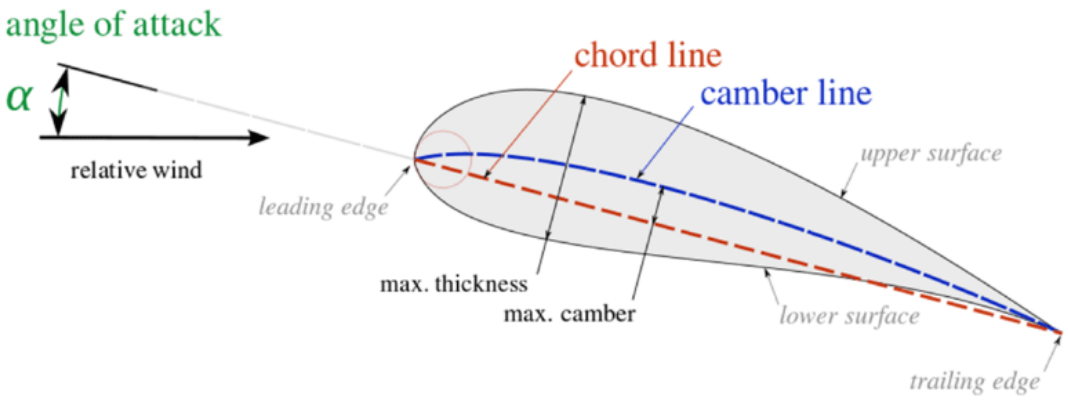

Figure 2: Airfoil Diagram (Chakraborty 2015)

Using either dimensions or coordinates in conjunction with these properties allow us to describe an airfoil.

The chord of an airfoil refers to the horizontal length of the airfoil from leading edge to trailing edge. The camber of an airfoil describes how much the profile of an airfoil curves away from the relative to the chord line. Most airfoils could be described as having a "teardrop" profile:

where the camber curves most across the upper surface. Airfoils where this is true for both upper and lower surfaces are referred to as symmetrical. The leading edge of an airfoil is the first point of the airfoil which contacts the air stream (or another fluid). The leading edge is defined using the Cartesian x,y coordinates (0,0). The trailing edge, therefore, is defined as the furthest horizontal position away from the leading edge on the physical airfoil. This position is expressed using the Cartesian coordinates (*n*, 0), where *n* is the horizontal distance from the leading edge, or the chord. The upper surface refers to series of coordinates that parallel a function defining the camber in the positive y direction. Similarly, the lower surface is expressed as a set of a coordinates following a function of the camber line in the negative y direction. Together these properties allow us to map an airfoil in 2 dimensions.

NACA series 4 uses these properties in a specific repeatably way to define airfoils in its group. NACA 4 series is referred to as such for the four digits used to describe each unique airfoil a part of it. The first digit of this series expresses the maximum amount of camber, that is curvature, as a percentage of the chord itself. That is the absolute value of maximum vertical distance of the camber line from the chord line divided by the chord. The second digit points to the position of that maximum vertical distance along a normalized chord (that is, the chord is expressed by a value of 1 or 100%). Consequently, this digit is an integer value greater than or equal to 1 and less than 10. Finally, the last two digits define the greatest thickness of the airfoil itself as a percentage of chord. This can be an integer value greater than 0 and less than 100. A NACA 4 series profile of 2405 would thus indicate that the airfoil would have a maximum curvature of 20% of the chord, with the position of the greatest point of curvature occurring at 40% of the way along the chord line from the leading edge. Finally, the general thickness of the airfoil would amount to 5% of the chord.

The process for selecting the airfoil defining the wing form involved first qualitative analysis followed by quantitative analyses separated into several iterative sections. In the qualitative analysis, the researcher reviewed material on optimal airfoils for gliding. Extending the flight time by combining powered horizontal cruise flight and unpowered horizontal gliding formed the rationale for selecting an airfoil optimized for gliding. Even though powered flight in the transverse direction could occur, the primary selection criteria was for gliding, as the drone would not be required to perform demanding aerial manoeuvres.

First, qualitatively, the researcher discovered that airfoils optimized for gliding were thinner airfoils with low profile curvature, or camber, and with the maximum camber occurring between the leading edge of the airfoil and about 50% of the total cross section. Consequently, three airfoils from each of the NACA 2300, 2400, and 2500 series were selected initially as

the matched the ideal qualities for the position of maximum camber for an airfoil intended for use in a gliding wing. From each series a thickness of 6%, 7%, and 8% were selected.

After an initial pool of airfoils was qualitatively selected, further analyses were conducted to determine which would be finally selected. This series of quantitative analyses was divided into three sub sections: 1) Preliminary Xfoil analysis 2) Excel analysis 3) Comparative Evaluation. The overall purpose of the analyses was to determine the optimal aerodynamic qualities obtainable at an optimal angle of attack. In theory, this would allow of the drone to achieve optimal glide characteristics.

First, each airfoil was individually evaluated across a range of angles of attack (α) in the aerodynamic analysis software Xfoil. It was observed that for the given airfoils, the lowest consistent value for alpha was -3°. Analyses of the airfoils in angles of attack lower that were than -3° frequently failed to converge. Trials were then run in 0.75° increments from -3° until a solution would no longer converge: indicating aerodynamic stall. Failure to converge could be seen as a wide turbulent separation of the boundary layer of airflow below the lower surface of the airfoil in negative α and above the upper surface of the airfoil in positive α.

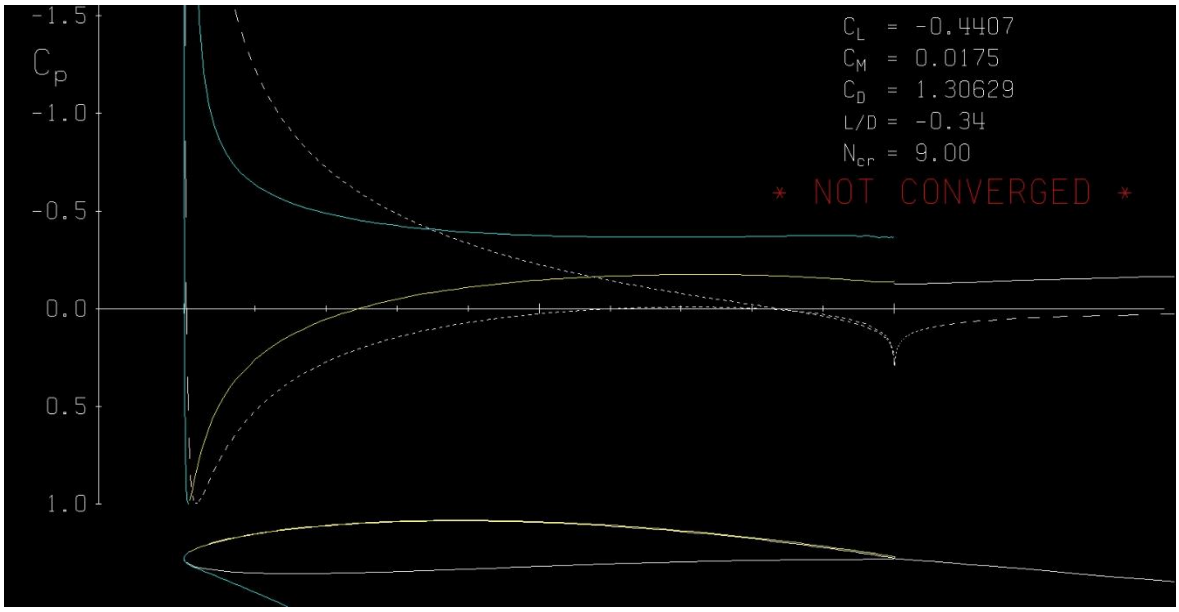

Figure 3: Xfoil Nonconvergent Analysis Example (Figure: Precious Akpata)

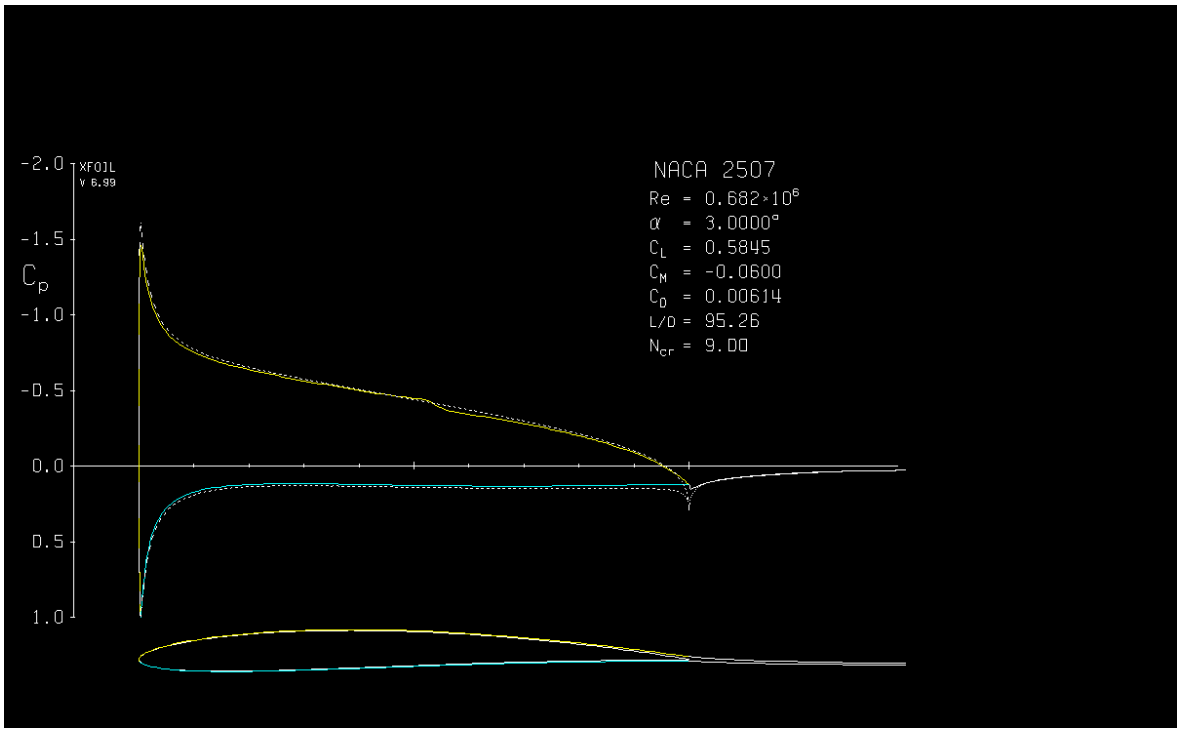

Figure 4: Xfoil Airfoil Analysis (Figure: Precious Akpata)

Trials most commonly ran in range from -3° to 4.5°. This analysis would produce initial results defining the coefficients of lift (C_L), drag (C_D), and moment (C_M) for a given angle of attack. These results were then tabulated together by NACA series, as shown in the figure below.

NACA 2506			
Alpha	CL	CD	CM
-3.00	0.5773	0.00654	-0.0592
-2.25	0.0038	0.00697	-0.0636
-1.50	0.1036	0.00571	-0.0679
-0.75	0.1788	0.00429	-0.0653
0.00	0.2711	0.00415	-0.0666
0.75	0.3504	0.00422	-0.065
1.50	0.4294	0.00442	-0.0635
2.25	0.5049	0.00506	-0.0612
3.00	0.5773	0.00654	-0.0592
3.75	0.6452	0.0094	-0.0574
4.50	0.7223	0.01085	-0.0561
5.25	0.7964	0.01283	-0.0543
6.00	0.8662	0.0161	-0.0516
6.75	0.9353	0.02139	-0.0485
7.50	3.8628	0.85959	-0.7105

NACA 2507			
Alpha	CL	CD	CM
-3.00	-0.0779	0.00784	-0.0637
-2.25	0.0217	0.0067	-0.0677
-1.50	0.1083	0.00573	-0.0684
-0.75	0.1835	0.00469	-0.0661
0.00	0.2729	0.00427	-0.0663
0.75	0.3526	0.00438	-0.0649
1.50	0.4322	0.00462	-0.0636
2.25	0.5094	0.00516	-0.0618
3.00	0.5845	0.00614	-0.06
3.75	0.6549	0.0081	-0.0582
4.50	0.7263	0.01021	-0.0566
5.25	0.8025	0.01159	-0.0552
6.00	0.8763	0.01328	-0.0535
6.75	0.9457	0.01572	0.0511
7.50	1.0117	0.01914	-0.0483
8.25	1.0765	0.02334	-0.0453
9.00	1.1283	0.02976	-0.041
9.75	4.1973	1.00249	-0.9465

NACA 2508			
Alpha	CL	CD	CM
-3.00	-0.0606	0.00754	-0.0677
-2.25	0.0262	0.00662	-0.0684
-1.50	0.1063	0.00585	-0.0675
-0.75	0.184	0.00508	-0.0658
0.00	0.2671	0.00446	-0.0643
0.75	0.3567	0.00458	-0.0653
1.50	0.4359	0.00484	-0.0639
2.25	0.5137	0.00531	-0.0624
3.00	0.5898	0.0061	-0.0607
3.75	0.6635	0.00737	-0.059
4.50	0.7334	0.00936	-0.0572
5.25	0.8066	0.01099	-0.0556
6.00	0.8813	0.01239	-0.0541
6.75	0.9542	0.01393	-0.01523
7.50	1.0228	0.01598	-0.0499
8.25	1.0877	0.0185	-0.0471
9.00	1.1516	0.0211	-0.0443
9.75	0.5565	2929497623	-0.0206

Figure 5: Xfoil Airfoils' Aerodynamic Data Comparison (Figure: Precious Akpata)

The second part of this iterative process involved taking the lift, drag, and moment coefficient data and further analysing them in a specific excel program (Hunsaker D 2023).

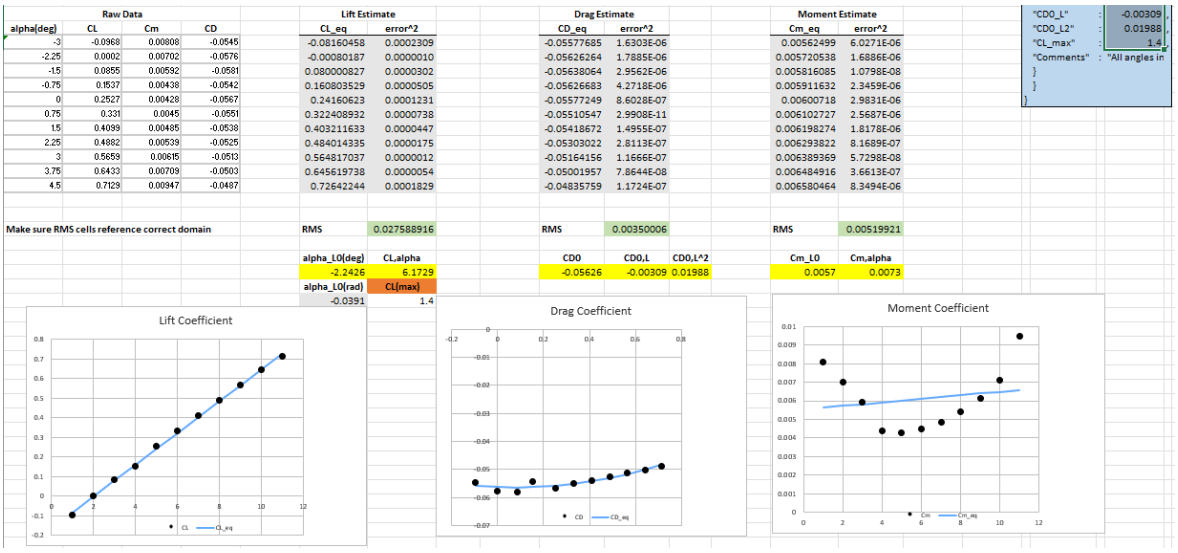

Figure 6: Excel Optmized Analysis (Excel Sheet Template: Hansaker D)

The aim of the sheet was threefold. First, to create an equation for each coefficient. Then by utilizing the excel solver to optimize the root mean square value it was possible to minimize the error between values delivered by the equation and values determined in Xfoil. Finally, this sheet produced further aerodynamic data to be evaluated using MachUp 5, an aircraft simulation application.

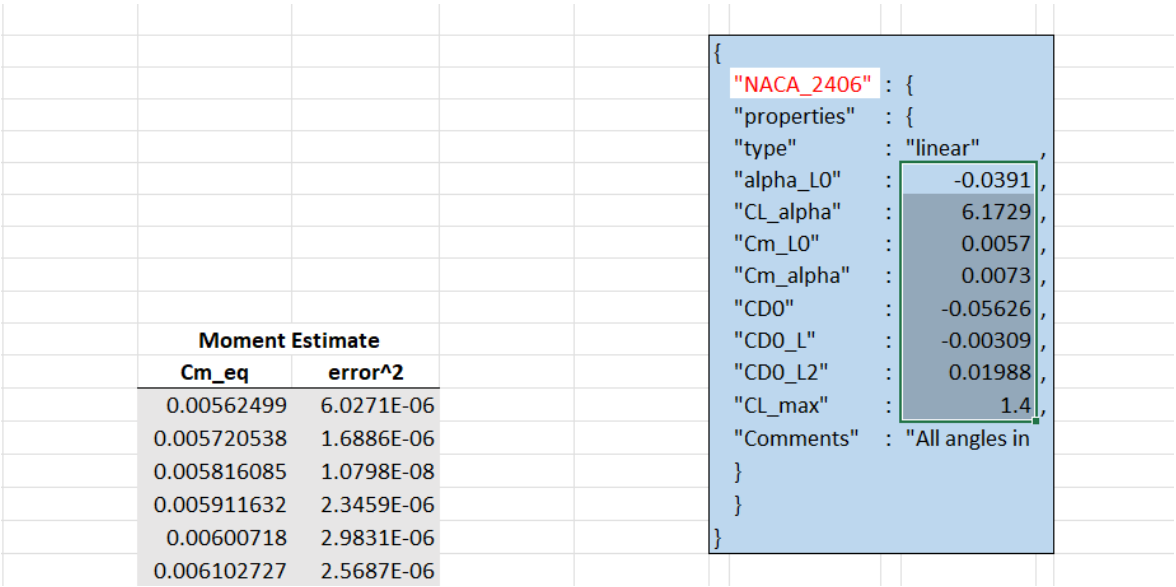

Figure 7: Excel Analysis Aerodynamic Properties (Excel Sheet Template: Hansaker D)

Similar to the first step using Xfoil, this second step using Excel was then repeated for each airfoil in each series and the results were tabulated together.

In the 3rd step, the results taken from Excel were then iteratively applied to a model of the lifting surfaces made in MachUp 5 and the gliding performance was run through two simulations. The first simulation, referred to as Target Lift, evaluated the weight of the UAV in conjunction with specific properties of a given airfoil (shown in the figure above) to find the optimal angle of attack for cruise flight. The second simulation, Forces and Moments, was used to calculate the forces and moments experienced by the craft during cruise flight. After all the iterations had been run, the researcher compared the results of all the airfoils, depicted in the figure below.

Table 1: Full Airfoil Comparison

Properties / NACA Profile	2306	2307	2308	2406	2407	2408	2506	2507	2508
Zero Lift AOA (Alpha) [rad]	-0.037	-0.0412	-0.0141	-0.0376	-0.0391	-0.0398	-0.0323	-0.0458	-0.0461
Coefficient Lift Slope [1/rad]	5.9246	5.6504	7.8626	6.232	6.1729	6.1893	10.0846	5.7598	5.81
Zero Lift Moment Coefficient	0.0029	0.0007	-0.0795	0.0057	0.0057	0.0059	-0.0554	0.0015	0.0028
Moment Slope [1/rad]	0.0896	0.111	1.4075	0.0113	0.0073	0.0039	1.6852	0.0935	0.0672
Zero Lift Coefficient of Drag	-0.04542	-0.04716	-0.06241	-0.09615	-0.05626	-0.05658	-0.07747	-0.0681	-0.0684
dCd/dL {Cd,L}	-0.01107	-0.00835	0.08229	-0.46432	-0.00309	0.06557	0.07555	0.00161	0.00595
d² Cd/dCl² {Cd,L²}	0.02541	0.02343	-0.04606	0.8625	0.01988	-0.08538	-0.06194	0.03257	0.01724
Clmax	1.4	1.4	1.4	1.4	1.4	1.4	1.4	1.4	1.4
Alpha From Target Lift [deg]	-693.3747	27.23	23.2357	32.1981	25.8542	25.4063	19.2021	26.7653	26.5364
FL [lbs]	7.2	7.2	7.2	7.2	7.2	7.2	7.207	7.2	7.2
FD [lbs]	1.1919	1.184	0.7127	14.0335	1.1328	0.2129	0.344	1.2953	1.126
FS [lbs]	-0.0711	-0.0716	-0.0682	-0.0753	-0.0704	-0.07	-0.0653	-0.0712	-0.071
MX [lbs*ft]	-0.003	-0.0031	-0.0027	-0.0038	-0.003	-0.0029	-0.0025	-0.0031	-0.003
MY [lbs*ft]	-1.5769	-1.6045	-1.1938	-1.8785	-1.5551	-1.5332	-0.993	-1.5834	-1.5776
MZ [lbs*ft]	0.0751	0.0757	0.0721	0.08	0.0744	0.074	0.0689	0.0752	0.075
Alpha From Target Lift [deg]	-693.3747	27.23	23.2357	32.1981	25.8542	25.4063	19.2021	26.7653	26.5364
FL [N]	32025.6	32025.6	32025.6	32025.6	32025.6	32025.6	32056.736	32025.6	32025.6
FD [N]	5301.5712	5266.432	3170.0896	62421.008	5038.6944	946.9792	1530.112	5761.4944	5008.448
FS [N]	-316.2528	-318.4768	-303.3536	-334.9344	-313.1392	-311.36	-290.4544	-316.6976	-315.808
MX [Nm]	-4.068	-4.2036	-3.6612	-5.1528	-4.068	-3.9324	-3.39	-4.2036	-4.068
MY [Nm]	-7014.0512	-7136.816	-5310.0224	-8355.568	-6917.0848	-6819.6736	-4416.864	-7042.9632	-7017.1648
MZ [Nm]	334.0448	336.7136	320.7008	355.84	330.9312	329.152	306.4672	334.4896	333.6

The decision was made to use NACA airfoil 2506. Airfoil 2506 was found to have the most reasonable angle α for target lift, out of tall the airfoils. It may have achieved a slight greater force of lift (F_L) than should have been possible; however, this may have been a minor error in the program execution. Alternatively, it may have been that at the given angle of attack, the airfoil would be able to generate slightly more lift than expected. It experienced the lowest drag force (F_D) and the least side slip force (F_S) of all the airfoils. When evaluating rolling (M_X), pitching (M_Y), and yawing (M_Z) moments, larger absolute values would result in greater stability, but less manoeuvrability. Values closer to zero would result in the contrapositive. Given that stability was seen as more important for the desired mission profile, the 2506 airfoil was not evaluated as the best of all the airfoils reviewed. Nonetheless, it was seen as reasonable. Its reasonable level of stability combined with good aerodynamic forces led to it being selected as the airfoil to be used. It should be noted that M_X and M_Y

are negative while M_Z is positive due to the application of coordinate system in the software. Further, the value for the angle α from target lift for airfoil 2306 was an error in the program.

3.5 Endurance and Range

Endurance was a key performance property that was focused on for the study, with aim of optimizing it. Range is a property linked to endurance and refers to the distance that an aircraft can travel. Range can be determined from the following.

$$R_{Max} = H\left(\frac{l}{d}\right)_{max} \tag{5}$$

Where *H* represents the given altitude and *l*/d represents the lift to drag ratio. When running simulations the lift force and drag force are frequently nondimensionalized and then expressed as the coefficient of lift to the coefficient of drag. In each case the absolute value of the ratio remains the same. Endurance refers to the time of flight for that range. Endurance is found using

$$E_{Max} = \frac{R}{V_s} \tag{6}$$

Where *R* is the range found in the previous equation and V_s is the velocity of descent or sinking speed.

While the two former equations provide a broad approach for determining the range and endurance of an aircraft, more specific equations were used in this study. The method used in this study worked to first solve for the endurance and then calculate the range. It was possible to solve for the E_{Max} given the following equation.

$$E_{Max} = \frac{\left(\left(\frac{Q_{Batt}}{1000}\right) \times N_{Batt} \times Ah_{used} \times \frac{1}{100}\right)}{\left(\frac{\left(I_{cruisedraw} + \left(P_{payload} + P_{avionics}\right)\right)}{v}\right)60} \tag{7}$$

Where,

Q_{Batt} = Battery Pack Capacity

N_{Batt} = Number of Batteries

Ah_{used} = Total Capacity Used

$I_{CruiseDraw}$ = Cruise Current Draw

$P_{Payload}$ = Payload Power

$P_{Avionics}$ = Avionics Power

v = Voltage = Number of Cells x Cell Voltage

From this it can be seen that the endurance of the drone was directly dependent several variables related to the drone's power source, in this a case a lithium polymer battery. Advancements in lithium polymer battery technology made it possible to select a battery of extremely high capacity (further detailed in section 3.6.2). In the case of this study, two batteries of 10 000 mAh each were selected. It was estimated that the total capacity used would 50%. While the payload and avionic power requirements were determined to be 10 W and 5 W, based on the selected LiDAR payload and other electronics. Finally, the voltage was found to total 30.4 v or 15.2 v per battery, given 8 cells and individual cell voltage of 3.8 v.

Indirectly, the endurance was also dependent on the total weight of the UAV, the area of the wings, and the aspect ratio of the wings. This can be viewed from the equation (8), equation (9), and equation (10), where g is gravity, $v_{aircruise}$ is cruise velocity, L/D is the lift to drag ratio, $\eta_{overall}$ is the overall efficiency, and η_{osw} is the Oswald efficiency. Additionally, C_{D0} and C_{df} represent the zero lift drag coefficient and fuselage drag coefficient respectively.

$$I_{CruiseDraw} = \left(\frac{\left(W_{Total} \times g \times v_{aircruise}\right)}{\frac{L/D}{v}} \right) \frac{100}{\eta_{overall}} \tag{8}$$

$$C_L = \frac{W_{Total} \times g}{\frac{1}{2}\rho (v_{aircruise})^2 S} \tag{9}$$

$$C_D = \frac{(C_{D0} + C_{df}) + (C_L)^2}{\pi \eta_{osw} AR} \tag{10}$$

Using equation (7) a maximum flight time of 79 minutes or approximately 1.3 hours was estimated. The range was then estimated to be 71.5 km from the following equation.

$$R_{Max} = \frac{60 \times T_{max} \times v_{cruise}}{1000} \tag{11}$$

3.6 Components

3.6.1 Initial Selection Criteria

Here we discuss the components of the LiDAR UAV that were not designed by the researcher, but rather selected to work together with the drone. It would be possible to construct approximately the same drone using different components. Given advancements in technology and improvements in product offerings, it could be seen as necessary to construct the drone using different components. Therefore, this section functions as a proof of concept. Most of the selected components were electronic in nature and thus not feasible to design from scratch for the scope of this thesis. The exception being the propellers, which were included in the selection group to help reduce complexity and increase reproducibility.

The primary metric, by which components were evaluated against, was weight. Given one of the chief aims of the research was LiDAR drone weight reduction, it followed that the weight of the selected components would need to be minimized as much as possible. The researcher was initially concerned that this could lead to performance trade-offs; however, overall, the selected components were able to meet the ideal specifications for the drone.

Table 2: Components List

Component Type	Component	Number Required	Individual Weight (g)	Σ Weight (g)
LiDAR Sensor	VLP 16 LiDAR Sensor	1	830.0	830.0
Propeller Motor	T-Motor F2203.5	4	19.7	78.8
Propeller	Master Airscrew G/F Series Propeller	4	26.1	104.4
Electronic Speed Controller	Hobbywing XRotor Micro 60A 6S 4-in-1 BLHeli32 ESC	1	15.0	15.0
Flight Controller	Flywoo GOKU GN745 F7 Flight Controller	1	8.5	8.5
Battery	Gens ace Advanced G-Tech 10000mAh 15.2V 100C 4S	2	930.0	1860.0
Radio Kit	HGLRC Hermes ExpressLRS Receiver Kit	1	1.0	1.0
Feed Camera	Runcam HD Zero Nano	1	6.0	6.0
Total	**Number of Components**	**15**		**2903.7**

3.6.2 Individual Selection Criteria

LiDAR Sensor

The VLP 16 Puck LiDAR sensor was selected for a number of reasons. Primarily, outside of weight considerations, the cost affected this decision. Given its comparatively high level of quality, its low cost was seen as highly advantageous. As mentioned in the introduction and section 3.6.1 the main considerations were time of flight and weight reduction. Nonetheless, it was seen as beneficial to design a LiDAR UAV with competitive flight times, low

weight, and low cost. This could expand the use of LiDAR mapping for fields of study and organizations where funding may be limited. As mentioned above, the VLP 16 was also seen as a reliable sensor, being one of the earliest general purpose LiDAR sensors released for the commercial market.

Two other LiDAR sensors were considered during the early selection process. They included the DJI Zenmuse L1 LiDAR and the Seed Studio TF03-100 Lidar. In terms of weight, the ideal selection would have been seen as the TF03-100, coming at only 89 g. This was followed by the VLP-16 at 830 g and lastly the Zenmuse at 930 g. In terms of LiDAR capabilities for aerial mapping, the order of the sensors was completely reversed. Thus, the VLP 16 was selected as it was in a set of three, neither the worst performing nor the best performing in each critical criterion.

Propeller Motors

There was a wide range of propeller motors to select from, even at very low weights. Therefore, the main criteria the researcher used to evaluate the motor selected was how well the motor could perform in relation to the propellers. Certain characteristics, detailed below, of the propellers were found to be critical to the overall performance of the UAV in flight. Matching the right motor to the propellers required due consideration.

Propellers

The propeller tip speed and diameter were found to be critical for performance optimization. Given the weight of the UAV was above 1000 g, it was necessary to select propellers with larger diameters that could maintain optimal tip speed. From figure 9 in appendix 2 a plot showing UAV weight to corresponding propeller diameters can be found. The weight of the UAV's components was found to be 1.2×10^3 g. The additional weight of the frame brought the weight up the approximately 1.5×10^3 g. This corresponded to a propeller diameter of 5 to 6 inches or 127 mm to 152 mm.

Battery

The battery pack was selected primarily for its exceptional capacity of 10 000 mAh. In addition to this the battery pack's weight (930 g) and physical dimensions (166 mm x 48 mm x 68 mm) were also optimal. A good battery was seen as having the properties of low to extremely low weight paired with medium to long life. The drone was designed to function with both hybrid fixed wing gliding and rotary capabilities. Consequently, the battery itself

did not necessarily have to provide high duration; however, it was viewed as useful in that it was capable of providing extended powered flight duration.

Communications and Other Electronics

A radio transmitter and receiver kit comprised the communications element of the drone. The other electronics selected included the Electronic Speed Controller, Flight Controller, and feed camera. For the scope of this research and the aims of the UAV design, these components were not focused on as much as others. The approach used for these components was to review the marketplace for competitive options and finding the components which could provide good performance at a low cost. The selected communications and other electronics, shown in table 2 above reflected these parameters.

3.7 Materials Selection

3.7.1 Concept

The principal concept that the materials selection process for the structural components was developed from was based on additive manufacturing. Specifically, the researcher aimed to ensure that the structural components that were required could be produced by 3D printing: making them more accessible to more people and also reducing the overall production costs. Stratasys, a company providing a wide range of specialized additive manufacturing products and services, proved to be a great source of information for the selection process. They provided some unique and high-end materials for the 3D printing process, such as Nylon 12 CF with exceptional chemical and physical properties. The other materials evaluated included regular Polylactic Acid (PLA) for 3D printing, ULTEM 9085, Essentium PEEK, and carbon fiber PLA.

3.7.2 Selection Criteria

To arrive at the decision for suitable structural material to be used in the construction of the frame, the researcher used a simplified Pugh approach for selection. In this approach each material was evaluated on two separate series of criteria: hard requirements and soft requirements. For each requirement a score of 1 (pass), 0 (neutral), and fail (-1) was given based on the criteria. The results of the selection criteria are shown below in table 3.

3.7.3 Materials Selection Evaluation

Table 3: Materials Evaluation

Material	PLA	Carbon Fiber PLA	Nylon 12 CF	ULTEM 9085	Essentium PEEK
Chemical Composition	$(C_3H_4O_2)_n$	$(C_3H_4O_2)_n$	$[(CH_2)_{11}C(O)NH]_n$	$(C_{37}H_{24}O_6N_2)_n$	$(-C_6H_4-O-C_6H_4-O-C_6H_4-CO-)_n$
Rigid Requirements					
Density (kg / m3)	1250	1300	1070	1340	1310
Evaluation	1	0	1	-1	-1
Strength (MPa)	37	45.5	63.4	47	92
Evaluation	-1	1	1	1	1
Melting Temperature (° C)	160	210	223	340	340
Evaluation	-1	0	1	1	1
Soft Requirements					
Price ($ / kg)	2.37	35	198,93	363,47	450
Price (€ / kg)	2,22	32.72	185,98	339,80	420,70
Evaluation	1	1	1	-1	-1
Accessibility	High	Medium	Medium	Medium	Low
Evaluation	1	0	0	0	-1
Sum Results	1	2	4	0	-1

The hard requirements were composed of physical properties necessary to make the structure stable. These requirements included density, tensile strength, and melting temperature. The density was used as a generalized expression of weight, as a consequence of how the materials were made available on the market. A lower the density corresponded to a lower weight and thus a higher score. A density of 1.3 x 10^3 kg / m^3 was selected as the neutral point. A higher density result in a negative evaluation and a lower density resulted in a positive evaluation. For strength, 45 MPa was selected as the neutral point; however, unlike with density, higher scores resulted in a pass and lower scores with a failure. Finally, melting temperature was assigned a neutral point of 200 °C. Similar to strength, higher scores were given a passing evaluation and lower scores a failing evaluation.

The soft requirements were separated into two main groups: price and accessibility. Price was evaluated on a quantitative scale where a lower value achieved a higher score. This decision was made to express affordability in a quantitative manner. Price was given in two forms: first in USD ($) and second in Euros (€). The reason for this was due to the primary currency that most materials were sold in. A uniform conversion rate was applied to the original price to express the quantities in Euros. This was seen as appropriate for the region in which the was being conducted. The last requirement was accessibility. This was more of a qualitative value, based on how easy it was to find suppliers for each material. Higher accessibility resulted in higher scores.

Each material was graded on a table against both all the requirements and each other. After each requirement an evaluation was given. Under all the requirements a sum total evaluation was calculated, based on the scores achieved in each requirement, by each material.

From the Material Selection Evaluation table, it can be seen that the material Nylon 12 CF achieved the highest score. This was somewhat surprising for the researcher, as initially it was expected that ULTEM 9085 or Essentium PEEK would achieve the highest score. This was not the case. Still, in the researcher's point of view, both of those materials could be seen as reasonably good for the purpose of constructing the frame. The second and third placed materials, PLA and Carbon Fiber PLA respectively, could also be seen as appropriate, if only from the perspective of cost and accessibility.

3.8 Challenges, Errors, and Limitations

This study was conducted over the course of 2 separate academic years, during three non-consecutive semesters. Consequently, certain initial observations and comparisons changed during the study. Particularly the cost and availability of certain components had to be slightly adjusted.

Additionally, it was the researcher's view that the study could have been narrower. After working through the paper, it was evident to the researcher that the most effective work done was focused on the wing sizing, airfoil analysis, and materials selection. It may have been a more focused study if only these factors were considered.

Furthermore, optimizing the flight time was both the most challenging and rewarding component of the study. In retrospect, this would have been the singular focus of the study, by way of the three former mentioned sections of work. Initially, it was the aim of the researcher to cover more areas. Work done revealed that depth of study would have been more effective than breadth.

4 Conclusion

The aim of this study was to find out the feasibility of producing a relatively lightweight, high endurance, and moderately low-cost LiDAR capable UAV. The study was able to demonstrate that a LiDAR drone capable of over an hour of sustained flight was possible. The study was almost able to reduce the weight to the optimal target; however, the results were 8% greater than desired. The mechanical outcomes are shown in the figure below.

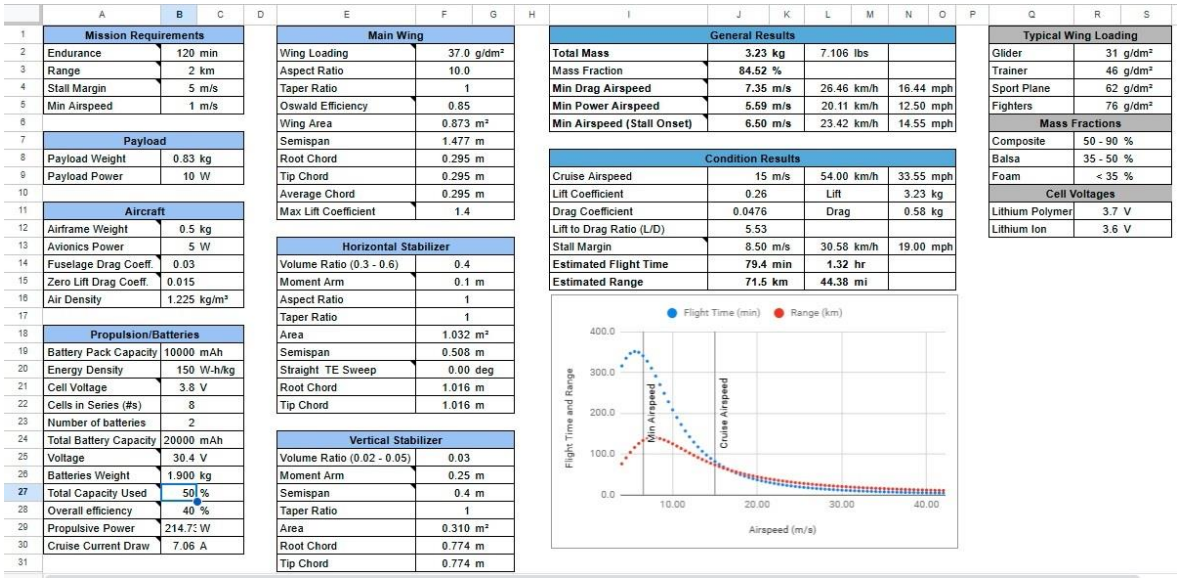

Mission Requirements	
Endurance	120 min
Range	2 km
Stall Margin	5 m/s
Min Airspeed	1 m/s

Payload	
Payload Weight	0.83 kg
Payload Power	10 W

Aircraft	
Airframe Weight	0.5 kg
Avionics Power	5 W
Fuselage Drag Coeff.	0.03
Zero Lift Drag Coeff.	0.015
Air Density	1.225 kg/m³

Propulsion/Batteries	
Battery Pack Capacity	10000 mAh
Energy Density	150 W-h/kg
Cell Voltage	3.8 V
Cells in Series (#s)	8
Number of batteries	2
Total Battery Capacity	20000 mAh
Voltage	30.4 V
Batteries Weight	1.900 kg
Total Capacity Used	50 %
Overall efficiency	40 %
Propulsive Power	214.73 W
Cruise Current Draw	7.06 A

Main Wing	
Wing Loading	37.0 g/dm²
Aspect Ratio	10.0
Taper Ratio	1
Oswald Efficiency	0.85
Wing Area	0.873 m²
Semispan	1.477 m
Root Chord	0.295 m
Tip Chord	0.295 m
Average Chord	0.295 m
Max Lift Coefficient	1.4

Horizontal Stabilizer	
Volume Ratio (0.3 - 0.6)	0.4
Moment Arm	0.1 m
Aspect Ratio	1
Taper Ratio	1
Area	1.032 m²
Semispan	0.508 m
Straight TE Sweep	0.00 deg
Root Chord	1.016 m
Tip Chord	1.016 m

Vertical Stabilizer	
Volume Ratio (0.02 - 0.05)	0.03
Moment Arm	0.25 m
Semispan	0.4 m
Taper Ratio	1
Area	0.310 m²
Root Chord	0.774 m
Tip Chord	0.774 m

General Results			
Total Mass	3.23 kg	7.106 lbs	
Mass Fraction	84.52 %		
Min Drag Airspeed	7.35 m/s	26.46 km/h	16.44 mph
Min Power Airspeed	5.59 m/s	20.11 km/h	12.50 mph
Min Airspeed (Stall Onset)	6.50 m/s	23.42 km/h	14.55 mph

Condition Results			
Cruise Airspeed	15 m/s	54.00 km/h	33.55 mph
Lift Coefficient	0.26	Lift	3.23 kg
Drag Coefficient	0.0476	Drag	0.58 kg
Lift to Drag Ratio (L/D)	5.53		
Stall Margin	8.50 m/s	30.58 km/h	19.00 mph
Estimated Flight Time	79.4 min	1.32 hr	
Estimated Range	71.5 km	44.38 mi	

Typical Wing Loading	
Glider	31 g/dm²
Trainer	46 g/dm²
Sport Plane	62 g/dm²
Fighters	76 g/dm²
Mass Fractions	
Composite	50 - 90 %
Balsa	35 - 50 %
Foam	< 35 %
Cell Voltages	
Lithium Polymer	3.7 V
Lithium Ion	3.6 V

Figure 8: General Results and Condition Results (Figure: Modified from Hansaker D Template Sheet)

The financial aim of the research was also met successfully, with the initial target to achieve a price lower than 7 000.00 €. A cost of 5 187.95 € was achieved. It should be noted that in principle the cost could be lower, as the drone did not require a full kilogram of Nylon 12 CF. Unfortunately, industrial 3D printing is not typically sold in units under 1 kg and so the minimum amount of material was used in the cost evaluation.

Table 4: Components and Material Costs

Component Type	Component	Number Required	Unit Weight (kg)	Unit Cost ($)	Unit Cost (€)	Total Cost	Total Cost (€)
LiDAR Sensor	VLP 16 LiDAR Sensor	1		4000	3800	4000	3800
Propeller Motor	T-Motor F2203.5	4		20	19	80	76
Propeller	Master Airscrew G/F Series Propeller	4		4	3.8	16	15.2
Electronic Speed Controller	Hobbywing XRotor Micro 60A 6S 4-in-1 BLHeli32 ESC	1		70	66.5	70	66.5
Flight Controller	Flywoo GOKU GN745 F7 Flight Controller	1		140	133	140	133
Battery	Gens ace Advanced G-Tech 10000mAh 15.2V 100C 4S	2		155	147.25	310	294.5
Radio Kit	HGLRC Hermes ExpressLRS Receiver Kit	1		20	19	20	19
Feed Camera	Runcam HD Zero Nano	1		75	71.25	75	71.25
3D Printing Material	Nylon 12 CF		1	750	712.5	750	712.5
Total	**Number of Components**	15		5234	4972.3	5461	5187.95

Based on the initial targets set in section 4.1 the study was almost successful, as two of the three aims were achieved.

Table 5: Outcomes

Performance Characteristic	Initial Aim	Results	Outcome
Weight (kg)	3	3.23	Fail
Flight Time (Hours)	1	1.32	Pass
Cost (€)	7000	5187.95	Pass

The researcher concluded that it would be possible to optimize modern LiDAR drones to have much higher endurance and lower costs than initially surveyed in the marketplace. As technology improves it is possible that costs may be reduced further. Weight reduction was also seen as feasible, although more difficult to achieve in conjunction with desired flight times. Overall, the study was able to demonstrate the present and future feasibility of LiDAR UAV weight reduction and optimization.

References

Bright, J., Rajkumar, S., Menon S, A. & Abimannan, G., 2020. Optimization of quadcopter frame using generative design and comparison with DJI F450 drone frame.

Carrio, A. et al., 2020. Onboard Detection and Localization of Drones Using Depth Maps. IEEE Access.

Chakraborty, M, 2015. A Computational Study on two horizontally close sequential airfoils to determine conjoined pressure distribution and aerodynamic influences on each other. Available at DOI:10.13140/RG.2.1.5041.4562

Durmus, S, 2020. Effects of Cubic Wing Loading Parameter on Airplane Wing Sizing and Parasitic Drag. J Aeronaut Aerospace Eng. 9:226

IMAGERY, U., 2017. Aerial Surveying: What is GPS, GNSS, RTK, PPK. [Online] Available at: https://www.uasimagery.com/map-accuracy-for-aerial-surveying/

Lohani, B. & Ghosh, S., n.d. Airborne LiDAR Technology: A Review of Data Collection and Processing Systems. Proceedings of the National Academy of Sciences, India Section A: Physical Sciences, Volume 87.

Menenti, M. & Zhien, W., 2021. Challenges and Opportunities in Lidar Remote Sensing. Frontiers.

Meyers, k, 2018. Wing Cube Loading (WCL). Ampeer. Retrieved on 23 November 2024. Available at https://www.sefsd.org/general-interest/wing-cube-loading-wcl/

MohamedZain , A. O. et al., 2022. Novel Drone Design Using an Optimization Software with 3D Model, Simulation, and Fabrication in Drone Systems Research.

Nvss, S. et al., 2022. Design and Development of Unibody Quadcopter Structure Using Optimization and Additive Manufacturing Techniques. Designs.

Zhang, K., Xie, J., Snavely, N. & Chen, Q., 2020. Depth Sensing Beyond LiDAR Range. IEEE.

Appendix 1: Market Analysis

4.1 Table 1. Preliminary Drone Market Comparative Analysis

Name	Ref 1	Ref 2	Cost ($)	Cost (€)	Weight (kg)	Max Taxoff Payload (kg)	Flight Time (Min.)	Dimensions (mm)	Rotors #	Airframe / Airfoil / Rotor Config	Cost / Weight	Cost / Weight
DJI M600 Pro lidar quadcopter	Link 1	Link 2	6,599.00	6,335.04	10.000	5.500	35	437 × 402 × 553	8	Multirotor	425.74	408.71
DJI M300 RTK	Link 1	Link 2	12,388.00	11,892.48	6.300	2.700		810 × 670 × 430	4	Multirotor	1376.44	1321.39
DJI Matrice 30 Series	Link 1	Link 2	9,999.00	9,599.04	3.770	0.228	36	470 × 585 × 215	4	Multirotor	2501.00	2400.96
DJI Matrice 200 Series	Link 1	Link 2	5,999.00	5,759.04	4.530	1.610	24	716 × 220 × 236	4	Multirotor	977.04	937.95
DJI Matrice 210 Series	Link 1	Link 2	10,410.00	9,993.60	4.570	1.570	24	716 × 220 × 236	4	Multirotor	1695.44	1627.62
Draganflyer Commander	Link 1	Link 2	14,999.00	14,399.04	2.750	1.000	25	873 x 873 x 295	4	Multirotor	3999.73	3839.74
Riegl RiCopter Lidar UAV	Link 1	Link 2			18.500	6.500	30	1,920 x 1,820 x 470	4	Multirotor	*0.00*	*0.00*
Riegl RiCopter M Lidar UAV	Link 1	Link 2			25.000	15.000	15	1,920 x 1,820 x 470	4	Multirotor	*0.00*	*0.00*
Harris H6 Hybrid	Link 1	Link 2	45,000.00	43,200.00	16.500	5.000	180		4	Multirotor	2093.02	2009.30
VulcanUAV Harrier Industrial	Link 1	Link 2			17.000	8.000	18	(D) 1150	8	Multirotor	*0.00*	*0.00*
Professional UAV KUR-1000HL	Link 1	Link 2	18,000.00	17,280.00	11.300	1.700	41		4	Multirotor	1384.62	1329.23
VelosUAV helicopter	Link 1	Link 2	3,705.00	3,556.80	10.000	10.000	60	(D) 1950	1	Helicopter	185.25	177.84
Robota Eclipse RTK	Link 1	Link 2	5,000.00	4,800.00	1.000	0.360	50	897.13 x 454.15 x 454.15	1	Fixed Wing	3676.47	3529.41
OnyxStar Xena drone lidar	Link 1	Link 2			3.600	2.000	37		8	Multirotor		
OnyxStar Fox-C8 HD quadcopter	Link 1	Link 2			6.000	3.000	34		8	Multirotor		
Tron F9 VTOL fixed wing lidar	Link 1	Link 2	53,900.00	51,744.00	11.500	2.000	90	3500 x 1800	2	Fixed Wing	3992.59	3832.89
Vapor 55 UAV helicopter	Link 1	Link 2			20.400	4.500	60	(D) 2291	1	Helicopter		
Yuneec H850-RTK Drone	Link 1	Link 2	6,266.95	6,016.27	5.800	3.000	65	440 × 365 × 470	6	Multirotor	712.15	683.67
Yuneec H520e Rtf	Link 1	Link 2	1,769.11	1,698.35	1.860	0.125	25	551 x 482 x 309	6	Multirotor	891.24	855.59
Average			14,925.77	14,328.74	9.494	3.884	47	**Mode**	4	Multirotor	1,115.73	1,071.11
No Information												
Optimal Flight Time			£27,217.99	£26,129.27								
Average												
Most Frequent Setup												

Appendix 2: Propeller Analysis

4.2 Figure 9: Propeller Diameter Analysis